Fracture and fatigue behavior of carbon/epoxy laminates modified by nanofibers

Mohammadi, Reza; Najafabadi, Mehdi Ahmadi; Saghafi, Hamed; Zarouchas, Dimitrios

DOI
10.1016/j.compositesa.2020.106015

Publication date
2020

Document Version
Final published version

Published in
Composites Part A: Applied Science and Manufacturing

Citation (APA)
Mohammadi, R., Najafabadi, M. A., Saghafi, H., & Zarouchas, D. (2020). Fracture and fatigue behavior of carbon/epoxy laminates modified by nanofibers. *Composites Part A: Applied Science and Manufacturing*, *137*, Article 106015. https://doi.org/10.1016/j.compositesa.2020.106015

Composites Part A 137 (2020) 106015

Contents lists available at ScienceDirect

Composites Part A

journal homepage: www.elsevier.com/locate/compositesa

Fracture and fatigue behavior of carbon/epoxy laminates modified by nanofibers

Reza Mohammadi[a], Mehdi Ahmadi Najafabadi[a,*], Hamed Saghafi[b,c], Dimitrios Zarouchas[d]

[a] Non-destructive Testing Lab, Department of Mechanical Engineering, Amirkabir University of Technology, Tehran, Iran
[b] Department of Mechanical Engineering, Tafresh University, Tafresh, Iran
[c] New Technologies Research Center (NTRC), Amirkabir University of Technology, Tehran, Iran
[d] Structural Integrity & Composites Group, Faculty of Aerospace Engineering, Delft University of Technology, Delft, the Netherlands

ARTICLE INFO

Keywords:
Composite laminates
Nylon 66 nanofibers
Fatigue loading
Mode-I fracture toughness

ABSTRACT

This research focused on fracture and fatigue response of carbon/epoxy laminates modified with electrospun nylon 66 nanofibers. For this purpose, AS4/8552 composite laminates interleaved by nanofibrous mat were considered under mode-I quasi-static and fatigue loading conditions. According to test outcomes, the fracture toughness increased about 133% under quasi-static tests. On the other hand, the plotted fatigue curves showed that the crack growth rate significantly decreased in modified samples and the threshold energy release rate enhanced about 128%. Finally, scanning electron microscopy (SEM) was also conducted to investigate the damage mechanisms.

1. Introduction

High-strength carbon/epoxy laminates are being applied in various industrial applications, such as automotive and aerospace structures. One of the most widespread matrices used in these type of materials is thermoset polymers like epoxy. Notwithstanding many advantages, such as low density and perfect mechanical performance, laminated composites can be delaminated easily under mechanical loadings which is because of the brittle nature of thermosets [1,2]. They can be failed by interlaminar cracks, which lead to the initiation of delamination and its propagation, resulting in final fracture.

Although the application of thermoplastics in the form of very thin film can be regarded as one of the most common toughening methods [3,4], the associated penalty of sacrificing the elastic modulus of the final product has limited their use in many industries [5]. Consequently, thermoplastic polymers in the form of nanofibers have gained rapid acceptance since 2001 which is introduced for the first time to increase fracture toughness of thermosets-based laminates [6]. High surface-to-volume ratio and high porosity of nanofibrous mat increased their capability in comparison with the film layers, and on the other hand remove their mentioned problem [7,8]. Various types of polymers, such as polysulfone [9,10], phenoxy [11], polyvinylidene fluoride [12,13], polyethersulfone (PES) [14,15], polyvinyl butyral [16,17], aramid [18], polycaprolactone [19–21], carbon [22–26] and nylon [15,27] have been applied as the toughener between composite layers, but the most attractive one is the latest, i.e. nylon [28].

Different types of nylon, i.e. 6, 66, and 69, have been used for toughening composite laminates [2,29,30]. Most researchers have focused on the nylon 66 and its effect during mode-I and mode-II fracture tests [29,31,32]. Brugo and Palazzetti [33] considered the influence nanomat thickness and also the laminate type, unidirectional or plain-woven, on fracture toughness. The outcomes showed that increasing the thickness led to enhancement of fracture toughness and, on the other hand, samples made of woven type were more affected by nanofibers. Gholizadeh et al. [32] investigated the effect of nylon 66 nanofibers on different damage modes using the acoustic emission method. The results showed that matrix cracking, debonding, and fiber breakage reduced about 82%, 53%, 64%, respectively, by interleaving nanofibers. Some researchers also conducted low-velocity impact tests on the reference and nanomodified laminates [2,34,35]. Akangah et al. [2] interleaved AS4/3501-6 composite laminates by nylon 66 and impacted under 0.46–1.8 J. According to the outcomes: threshold impact force increased about 60% and the rate of impact damage growth rate decreased to one-half with impact height. In another study, Saghafi et al. [35] conducted tests on the curved glass/epoxy laminates. Their results showed adding nanofibers did not change impact parameters like maximum load and displacement, but could reduce the delaminated area significantly (about 60%).

Although many papers have been published regarding fracture and impact behavior of nanomodified laminates, the study about fatigue

* Corresponding author.
E-mail address: ahmadin@aut.ac.ir (M.A. Najafabadi).

https://doi.org/10.1016/j.compositesa.2020.106015
Received 3 March 2020; Received in revised form 20 April 2020; Accepted 9 June 2020
Available online 26 June 2020
1359-835X/

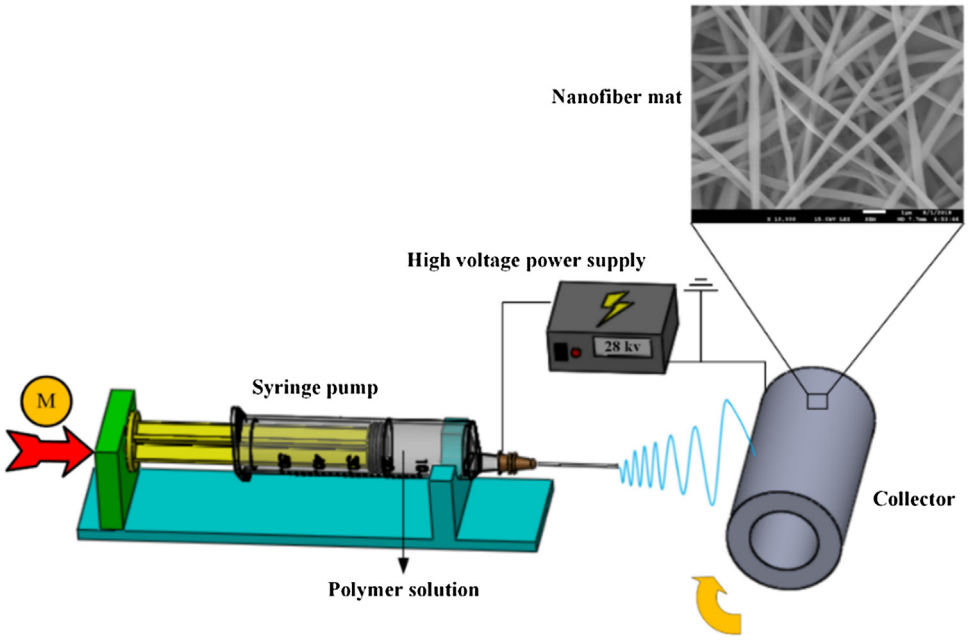

Fig. 1. Schematic picture of the electrospinning process. (For interpretation of the references to colour in this figure legend, the reader is referred to the web version of this article.)

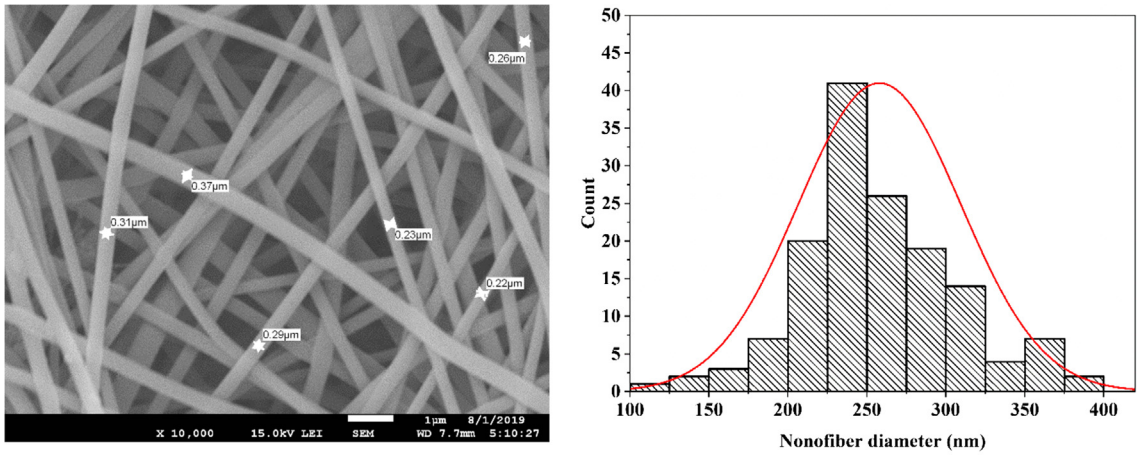

Fig. 2. A) SEM image of nanofibers **B)** fiber diameter distribution. (For interpretation of the references to colour in this figure legend, the reader is referred to the web version of this article.)

response of these laminates is very limited [36–38]. For instance, Polat et al. [36] examined the influence of graphene nanoplates/nylon 66 nanofiber mats on the fatigue life of composite to aluminum single-lap joint. The tests were done with various maximum stress levels as 20%, 30%, 40%, 50% and 60% of breaking shear tensile strength, and the results showed that the nanomaterial could increase the life cycle incredibly. In this study, pure nylon 66 nanofibers are used as the toughener of carbon/epoxy to consider the toughening mechanism under mode-I fracture and fatigue loadings. The fatigue tests were conducted under constant displacement ratio and various ratios of fracture toughness, (G_{Iimax}/G_{IC}). On the other hand, the aim is to assess the constant crack growth rate section of the Paris law diagrams for the reference and nanomodified specimens and also determining physical strain energy release rate (G*) for both samples. Finally, scanning electron microscope (SEM) was applied for investigating the fractured surface of laminates.

2. Manufacturing specimens

2.1. Electrospinning method

In order to produce nanofibers, the electrospinning method was applied. Fig. 1 shows the schematic picture of the electrospinning apparatus and its process. The electrospinning setup consists of four major components namely, high voltage power supply, a syringe with metal needle, injection feed rate system, and a conductive collector. By applying a high voltage electric field between needle and collector, the polymer solution is wrapped around the collector as nanofibers. To obtain nylon 66 nanofibers, the main process parameters such as applied voltage, collector rotational speed, and injection feed rate were selected 28 kV, 100 rpm and 0.8 mL/h, respectively. In this research, the nylon 66 provided from DuPont Company, and formic acid (FA) and 2.2.2-Trifluoroethanol (TFE) solvents purchased from Merck Company. The solution was prepared by adding 20% w/v nylon 66 pellets in the solvents of (FA/TFE) with the ratio of 30/70 v/v. The final produced

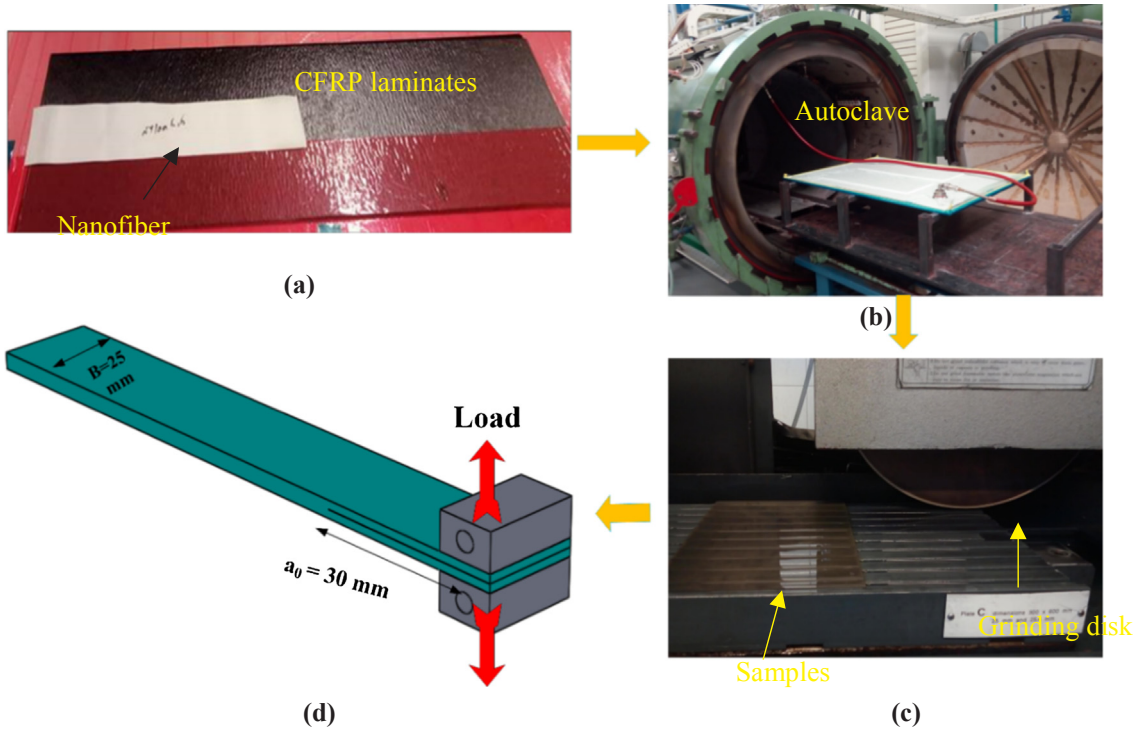

Fig. 3. The steps of fabrication and loading condition: **A)** laminating of prepreg **B)** curing in autoclave **C)** cutting with grinding machine **D)** schematic of mode-I loading. (For interpretation of the references to colour in this figure legend, the reader is referred to the web version of this article.)

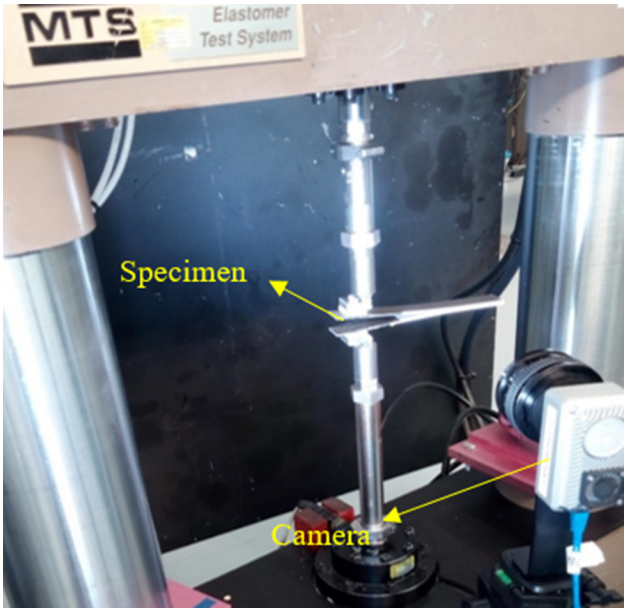

Fig. 4. Mode-I test setup. (For interpretation of the references to colour in this figure legend, the reader is referred to the web version of this article.)

nanomat was 7.5 gr/m^2 weight per area (50 μm thickness) and had a porosity of 87%. Thermal characterization of nylon 66 is also an important factor to understand the mechanism applied by nanofibers to toughen the laminates: melting point: 260 °C and T_g temperature: 55 °C [39]. On the other hand, Papadopoulou [40] used TGA data to prove that nylon 66 nanofibers have very good thermal stability until 300 °C (< 5% mass loss) and the major thermal degradation was after 350 °C.

SEM image of produced nanofibers and their diameter distribution were depicted in Fig. 2. The diameters were measured by investigating 150 fibers using an image analysis software (ImageJ). As seen in Fig. 2-

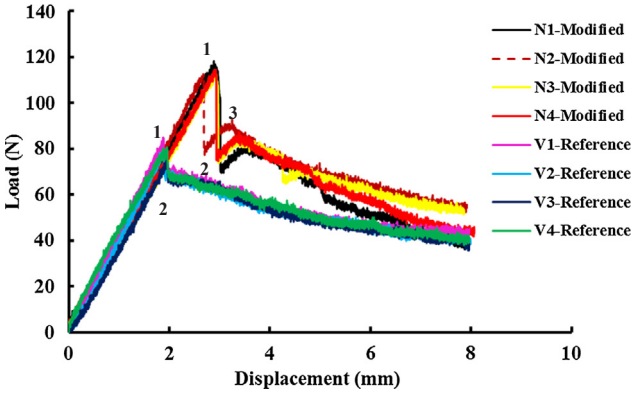

Fig. 5. Load-displacement curves for the reference and modified specimens under quasi-static mode-I loading. (For interpretation of the references to colour in this figure legend, the reader is referred to the web version of this article.)

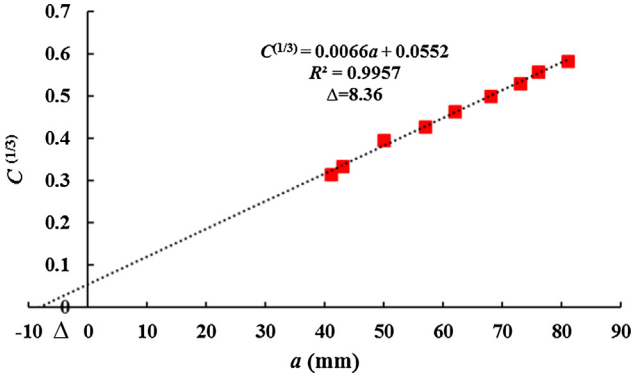

Fig. 6. The linear relationship between crack length and the third root of compliance. (For interpretation of the references to colour in this figure legend, the reader is referred to the web version of this article.)

Table 1
Test parameters and fracture toughneses values for all quasi-static specimens.

Specimen codes	a_0 (mm)	B (mm)	δ_{cr}	P_{cr} (N)	Δ (mm)	G_{IC} (kJ/m^2)	P_{cr} (Ave.)	Δ (Ave.)	G_{IC} (Ave.)
V1	40	25.07	1.87	84.77	8.36	0.196	79.72	10.40	0.181 ± 0.014
V2	40	25.09	1.88	79.21	9.69	0.179			
V3	40	25.1	1.94	74.58	13.33	0.162			
V4	40	25.01	1.95	80.6	10.22	0.187			
N1	40	25.09	2.88	118.13	6.75	0.435	114.42	6.04	0.423 ± 0.013
N2	40	25.06	2.67	112.57	3.71	0.411			
N3	40	25.07	2.92	112.57	7.83	0.411			
N4	40	25.1	2.9	114.43	5.89	0.432			

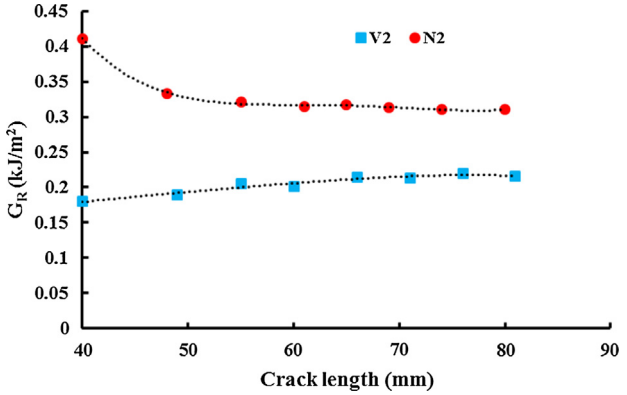

Fig. 7. Delamination resistance curve for V2 and N2 specimens. (For interpretation of the references to colour in this figure legend, the reader is referred to the web version of this article.)

Table 2
The characteristics of fatigue tests specimens and procedure.

specimen	a_0 (mm)	Width (B) (mm)	Thickness (h) (mm)	G_{IImax}/G_{IC}	δ_{max} (N)	δ_{min} (N)
V5	40	25.07	4.57	0.8	1.79	0.54
V6	40	25.08	4.56	0.7	1.66	0.5
V7	40	25.06	4.59	0.5	1.4	0.42
V8	40	25.09	4.55	0.8	1.79	0.54
N5	40	25.06	4.58	0.8	2.6	0.78
N6	40	25.08	4.57	0.7	2.4	0.72
N7	40	25.05	4.58	0.5	2.03	0.61
N8	40	25.08	4.56	0.8	2.6	0.78

B, the range of diameter is distributed between 100 and 400 nm. The mean value of normal distribution is about 260 nm.

2.2. Laminating process

Fig. 3 shows the steps of specimen fabrication and loading conditions. The AS4/8552 carbon/epoxy prepreg was employed for the laminating and fabricating of composites plates. The 24 prepreg layers were used for stacking and during the laminating process, a 12.7 μm-Teflon film was implanted between mid-plies to create an initial pre-crack. Nanofibrous mat was firstly dried at a vacuum oven and then put at front of the Teflon layer as seen in Fig. 3-A.

In order to eliminate some fabrication errors and to have a similar condition during the laminating and curing process, both the reference and modified specimens were provided from the same palate. After laminating, the plate was placed in an autoclave (Fig. 3-B) to cure according to the datasheet [41]. The heating rate was fixed at 1 °C/min. The panel was cut to 175 mm length and 25 mm width using a grinding machine (Fig. 3-C). Then, aluminum block attached to end of the samples using superglue in order to apply force by machine. Finally, the specimens were tested under mode-I loading (Fig. 3-D).

3. Quasi-static fracture tests

The fracture tests were conducted according to ASTM D5528 [42] using Double Cantilever Beam (DCB) specimens. The fracture specimens were loaded under displacement control with constant displacement rate, 1 mm/min. The values of load and displacement were continuously measured and the crack length was also recorded using a digital camera (Fig. 4). Four samples for each type of specimens were tested to investigate the repeatability. V and N represent the reference and nanomodified laminates, respectively, in the text and figures.

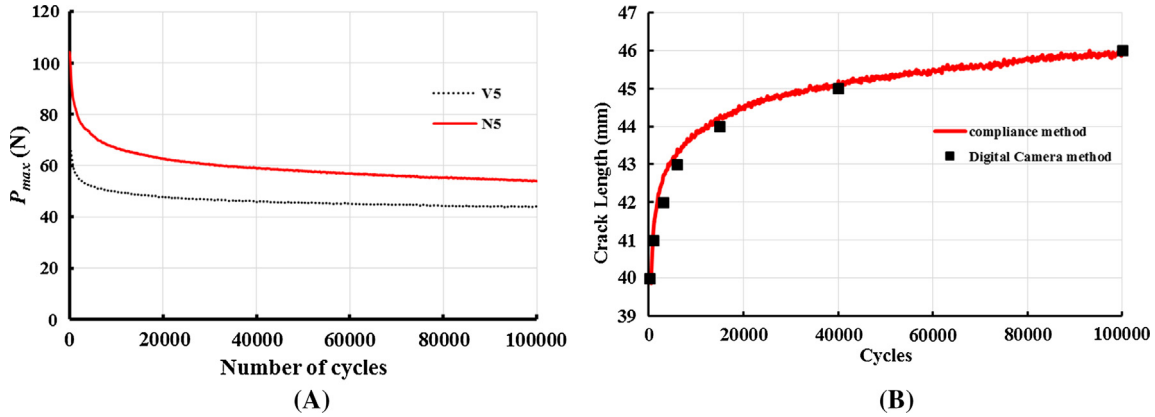

Fig. 8. A) Decrease in maximum load during cycles. **B)** Increase of crack length per cycle and verification of compliance method with the visual method. (For interpretation of the references to colour in this figure legend, the reader is referred to the web version of this article.)

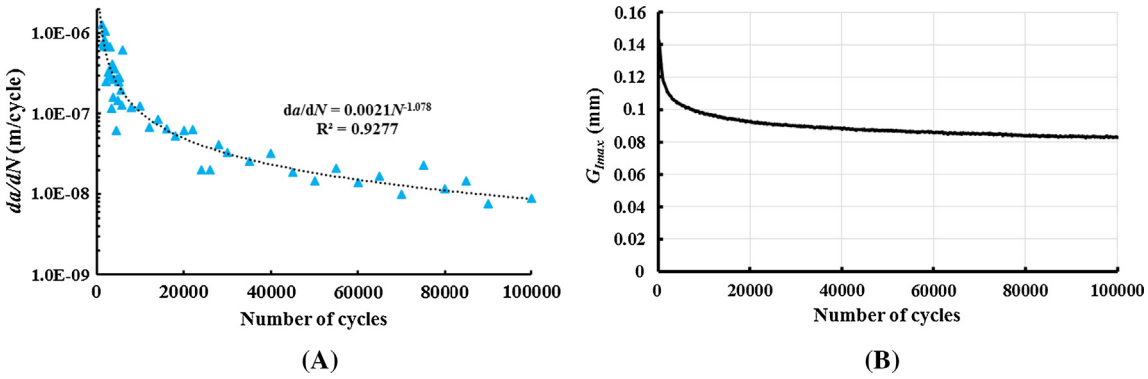

Fig. 9. Decrease of: **A)** crack growth rate and **B)** maximum energy release rate versus number of cycles. (For interpretation of the references to colour in this figure legend, the reader is referred to the web version of this article.)

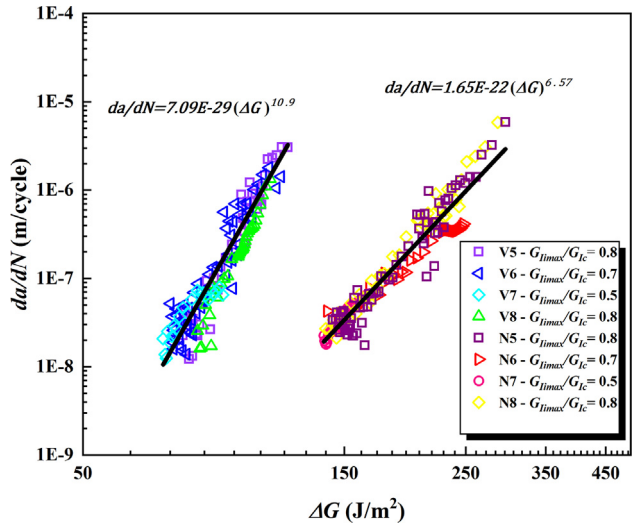

Fig. 10. Fatigue crack growth rate vs. ΔG for all reference and nanomodified specimens. (For interpretation of the references to colour in this figure legend, the reader is referred to the web version of this article.)

3.1. Quasi-static results

Load-displacement curves of the reference and nanomodified laminates tested under quasi-static conditions are shown in Fig. 5. As seen, the slope of curves is the same for all samples before crack propagation which proves the presence of nanofiber does not affect the slope. When the load reached the maximum load (p_{cr}) (Point **1**), the crack started to propagate. The maximum load corresponds to 79.7±4.2 N and 114.4±2.6 N for the reference and modified laminates, respectively, which shows 44% enhancement. Then, because of the resin-rich area at initial delamination tip, a big drop occurred in the load which represents the crack length increased suddenly (Point **2**). This force drop is significantly more in the nanomodified sample which is because of this fact that the presence of nanofibers caused further rise of p_{cr}. Therefore, more stress is in front of the crack tip in the nanomodified laminate. When the nanofibers could not withstand more stress, higher amount of energy released in the modified laminate in comparison with the reference. After Point **2**, the curve trend of the reference and modified laminates are different. The nanofibers were again active and so the force increased until Point **3**.

€According to ASTM-D5528 standard, Eq. (1) is applied for obtaining mode-I interlaminar fracture toughness (G_{IC}):

$$G_{IC} = \frac{3p_{cr}\delta_{cr}}{2B(a_0 + \Delta)} \quad (1)$$

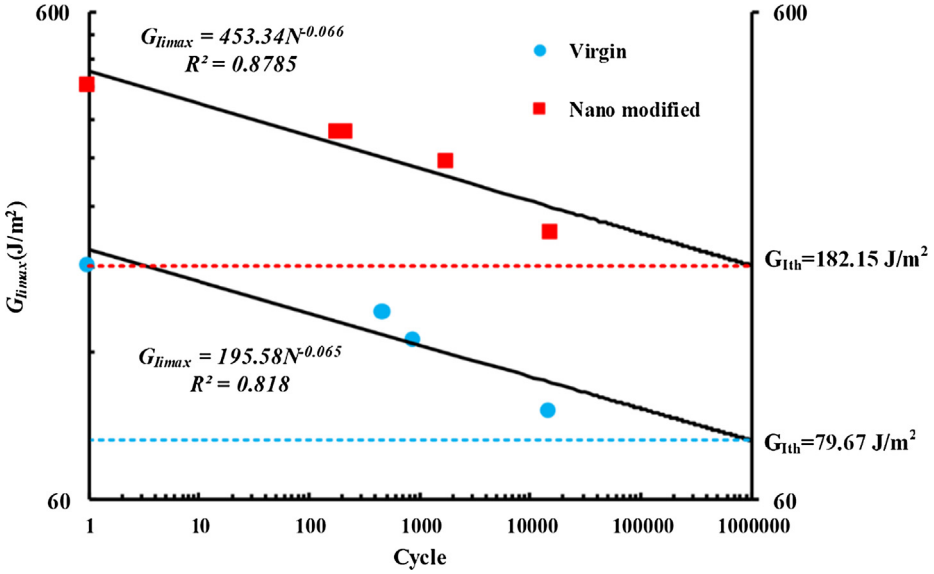

Fig. 11. Determining the threshold energy release rate (G_{Ith}) for the reference and modified specimens. (For interpretation of the references to colour in this figure legend, the reader is referred to the web version of this article.)

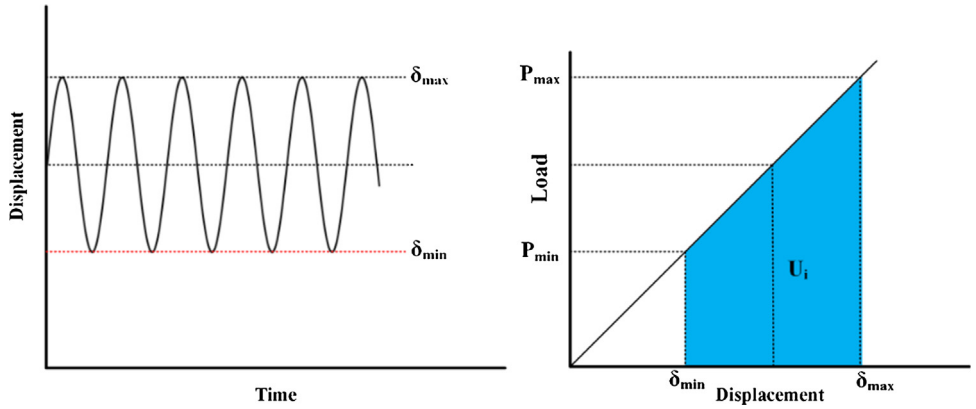

Fig. 12. The method of calculating potential energy at each cycle. (For interpretation of the references to colour in this figure legend, the reader is referred to the web version of this article.)

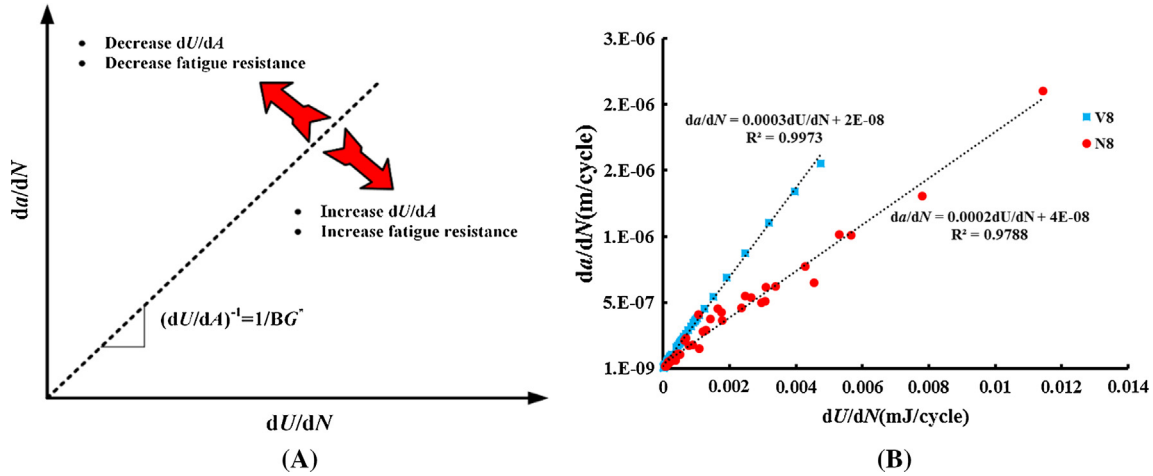

Fig. 13. A) The relationship between G^* and fatigue resistance **B)** da/dN - dU/dN graph for the reference and modified specimens. (For interpretation of the references to colour in this figure legend, the reader is referred to the web version of this article.)

where p_{cr} is the maximum force, δ_{cr} is the displacement corresponding to p_{cr}, a_0 is the initial crack length (40 mm), B is the specimen width (25 mm) (Fig. 3-D) and Δ is the crack length correction. According to the ASTM D5528 standard, the Δ parameter is determined experimentally by generating a least squares plot of the cube root of compliance ($C^{1/3}$) as a function of delamination length. The compliance, C, is the ratio of the load point displacement to the applied load, δ/P. As an example, Fig. 6 shows the linear relationship between crack length and third root of compliance and the value of Δ for V1 specimen.

Table 1 shows the mode-I fracture toughness values and other main parameters for all fracture test specimens. As it can be seen, the average of G_{IC} is 0.181 ± 0.014 kJ/m^2 and 0.423 ± 0.013 kJ/m^2 for the reference and modified specimens, respectively, which shows 133% increase of fracture toughness by adding nanofibers. Delamination resistance curve (R-curve) was also plotted in Fig. 7. As seen, all G_R values for the modified specimen are significantly more than the reference one (53% increase in the average values).

4. Fatigue test procedure

ASTM D6115 [43] standard was employed to conduct fatigue tests. According to this standard method, specimens were tested under the sinusoidal cyclic loading condition at a frequency of 5 Hz and a cyclic displacement ratio $R = \delta_{min}/\delta_{max} = 0.3$. Eq. (2) was used for obtaining of maximum displacement (δ_{max}) for G_{Iimax}/G_{IC} ratios of 0.5, 0.7, and 0.8.

$$\frac{G_{Ii\max}}{G_{IC}} = \left(\frac{\delta_{\max}}{\delta_{cr}}\right)^2 \tag{2}$$

where G_{IC} is the mode-I fracture toughness which is 0.181 and 0.423 kJ/m^2 for the reference and modified specimens, respectively. G_{Iimax} is the maximum Strain Energy Release Rate (SERR) during the first cycle. According to Table 2, the values of δ_{cr} are 1.91 ± 0.04 mm and 2.84 ± 0.11 mm for the reference and nanomodified specimens, respectively. The values of displacement, load, and cycle count were recorded at each cycle during the fatigue test. These data were used to plot all fatigue curves. Each specimen was tested until $N = 100000$ cycles.

4.1. Fatigue test results

Due to displacement - control condition, δ_{max}, and δ_{min} were constant during the cyclic test while P_{max} and P_{min} continuously decrease with increasing the number of cycles. Fig. 8-A shows this matter for N5 and V5 specimens. In order to calculate the crack length during the fatigue test, the compliance method was applied. In this method, compliance (δ_{max}/P_{max}) is calculated at each cycle, then crack length is achieved using the relation mentioned in Fig. 6. Fig. 8-B illustrates the calculated crack length (a) using this method and digital camera technique. As seen, there is good agreement between these two methods.

According to ASTM E647 [44], da/dN is determined from Eq. (3):

$$\left(\frac{da}{dN}\right)_i = \frac{a_{i+1} - a_i}{N_{i+1} - N_i} \tag{3}$$

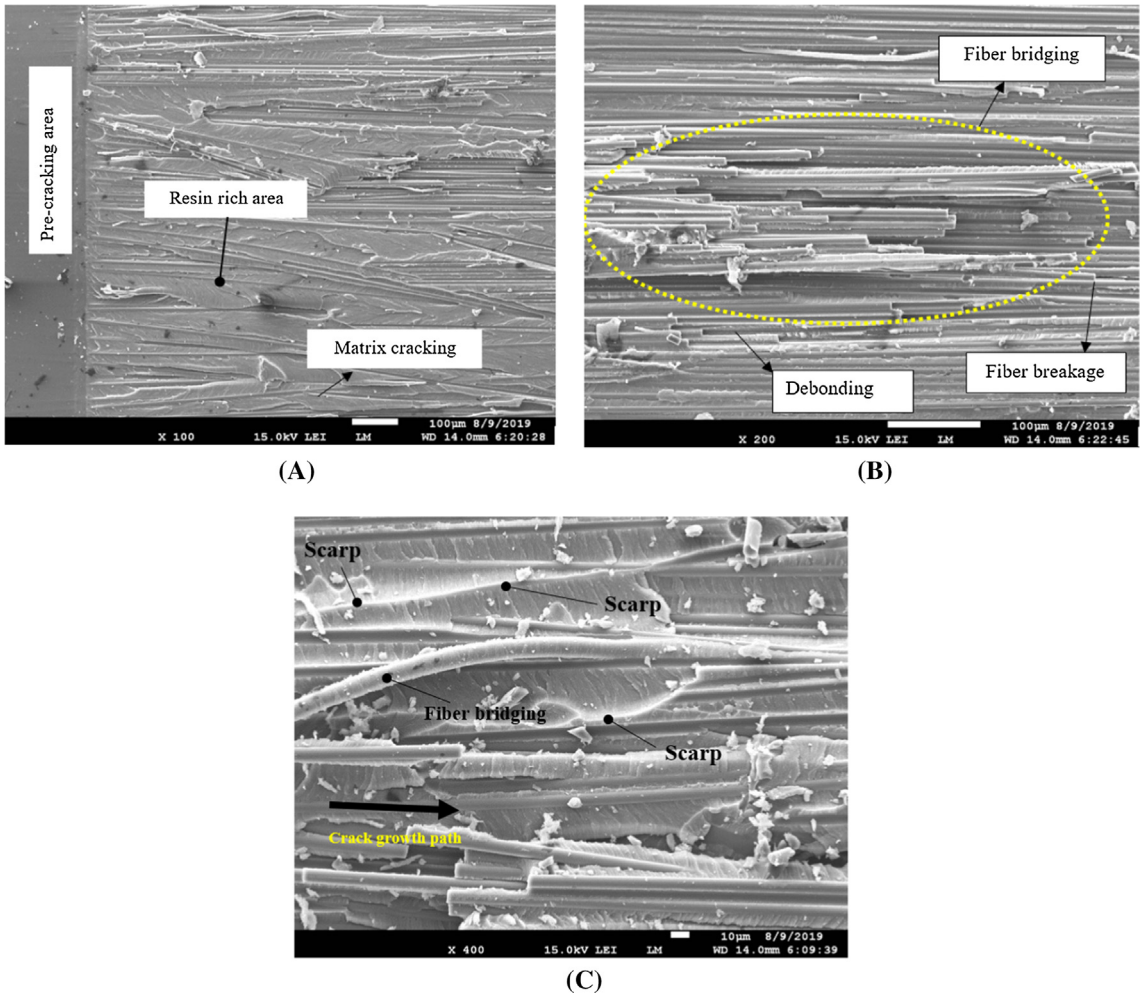

Fig. 14. The fractured surface of reference specimens under quasi-static test **A)** Resin rich area near the initial crack tip **B)** fiber bridging phenomenon occurred away from the initial crack tip. **C)** making scarp during matrix cracking in the reference laminates. (For interpretation of the references to colour in this figure legend, the reader is referred to the web version of this article.)

where a_i and N_i are the crack length and cycle count. a_{i+1} is the next available data point and N_{i+1} is the cycle count corresponding to a_{i+1}. The maximum SERR (G_{Imax}), the minimum SERR (G_{Imin}), and the SERR range (ΔG) in the current cycle are obtained from Eq. (4), (5), and (6), respectively.

$$(G_{\mathrm{Im}ax})_i = \frac{3(p_{\max})_i \delta_{\max}}{2B(a_i + \Delta_{ave})} \tag{4}$$

$$(G_{Imin})_i = \frac{3(p_{\min})_i \delta_{\min}}{2B(a_i + \Delta_{ave})} \tag{5}$$

$$\Delta G = (G_{I\max})_i - (G_{I\min})_i \tag{6}$$

where Δ_{ave} is the average of crack length correction parameter achieved from quasi-static tests (See Table 1). Fig. 9 illustrates the crack growth rate (da/dN) and the maximum energy release rate (G_{Imax}) vs. cycle for V5 specimen. As shown, with increase of cycles both parameters decreased. Note that Fig. 9-A has been drawn at a log-linear scale (Y-axis is a logarithmic scale).

Fig. 10 presents da/dN versus ΔG in the logarithmic scale. As observed, da/dN decreased when the reference and nanomodified laminates tested under a constant ΔG. A typical Paris law can be established between the crack growth rate and ΔG values as follows:

$$\frac{da}{dN} = \alpha(\Delta G)^n \tag{7}$$

where α and n can be calculated by fitting a curve on experimental data (Fig. 10). The n values for the reference and nanomidified laminates are 10.9 and 6.57, respectively, which shows the presence of nylon 66 could decrease the slope of the da/dN- ΔG curve. With a quick glance at this figure, it is obvious that the crack growth rate is significantly more in the reference laminates. Another point regarding this figure is that the curves of nanomodified specimens transfer to the right. It means that modified laminates require more ΔG for propagating the crack with the same da/dN value. As an example, using Paris relationship, ΔG values corresponding to da/dN = 1e-6 m/cycle, are 107 J/m^2 and 252 J/m^2 for the reference and modified specimens, respectively, which means modified specimen has 135% more resistance to crack growth, and can be loaded with higher ΔG values.

In this study, to find out the number of cycles (N) for the start of delamination, the suggestion of ASTM standard D6115 was used. According to this standard, the number of cycles corresponding to 5% enhancement of the compliance was applied to establish the delamination onset life ($N_{5\%}$). G_{Imax} vs. $N_{5\%}$ is presented in Fig. 11. The G_{Imax}-$N_{5\%}$ relationship is often shown by the following equation [45]:

$$G_{Imax} = DN_{5\%}{}^k \tag{8}$$

where D and k can be obtained by fitting a curve on experimental data. The threshold energy release rate (G_{Ith}) was calculated using the Eq. (6) when $N = 10^6$ cycles. Hence, G_{Ith} is 79.67 J/m^2 and 182.15 J/m^2 for the reference and nanomodified specimens, respectively, which shows

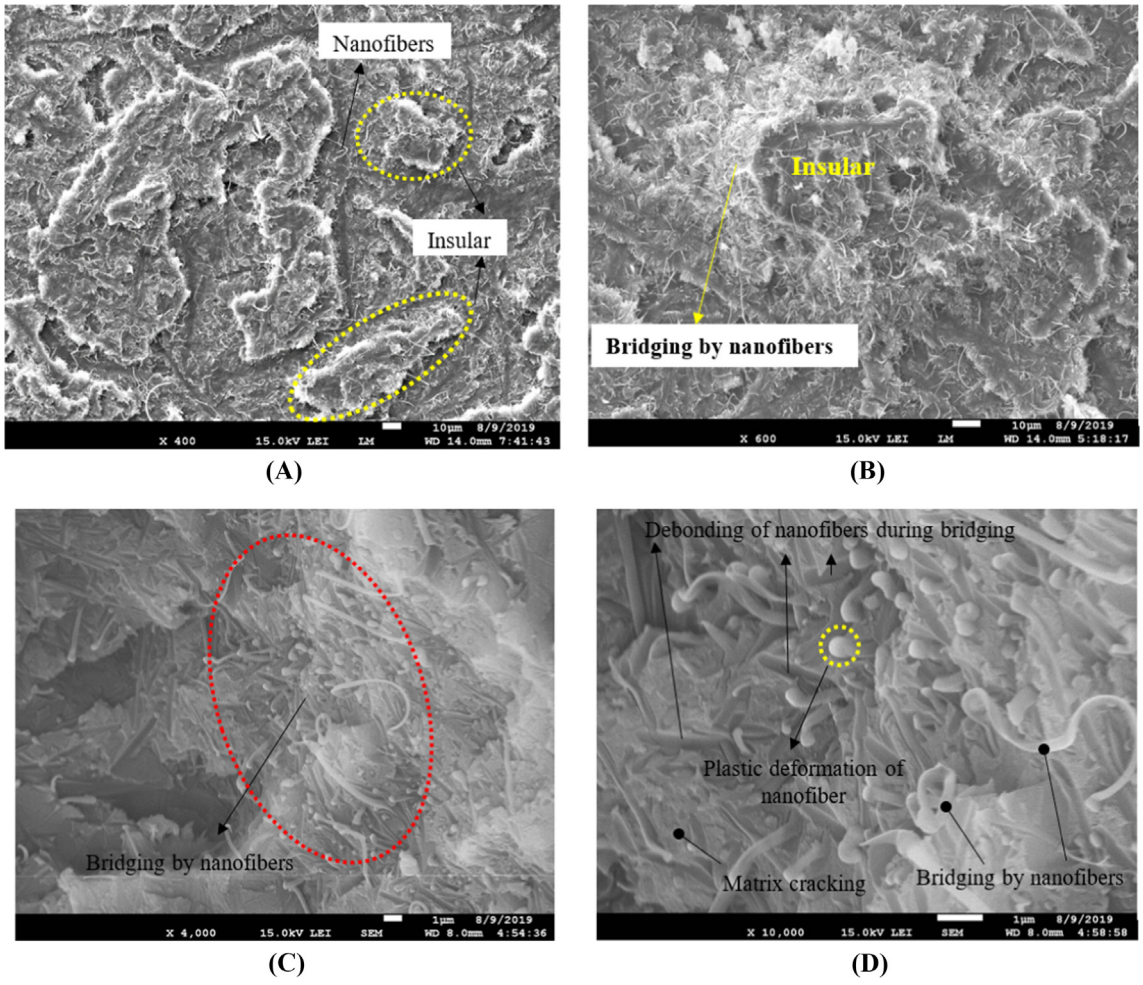

Fig. 15. The fractured surface of nanofiber-modified specimens under quasi-static test. (For interpretation of the references to colour in this figure legend, the reader is referred to the web version of this article.)

128% enhancement.

5. Physical strain energy release rate method

Some researchers [46,47] have used physical strain energy release rate (PSERR, called by G^*) to assess fatigue resistance of composite materials. This parameter is the actual strain energy release rate that achieved from measured data, not from the theoretical method. Eq. (9) is used to calculate the G^*:

$$G^* = \frac{1}{B}\frac{dU/dN}{da/dN} = \frac{dU}{dA} \tag{9}$$

where U is the potential strain energy and dU/dN is the dissipation of the potential energy rate per cycle obtained from Eq. (10):

$$\frac{dU}{dN} = \frac{U_{i+1} - U_i}{N_{i+1} - N_i} \tag{10}$$

where U_i and U_{i+1} are the potential energy at ith and $i + 1$th cycle, respectively, calculated using Eq. (11) and Fig. 12:

$$U_i = \frac{1}{2}(P_{max} + P_{min})_i(\delta_{max} - \delta_{min}) \tag{11}$$

According to Eq. (9) and Fig. 13-A, with decrease of the slope in da/dN - dU/dN curve, the G^* value increased; so, the fatigue resistance became more. Fig. 13-B shows the da/dN - dU/dN plot for both of the reference and modified specimens. As seen, there is a linear relationship between da/dN and dU/dN parameters. Since the G^* is the inverse slope of the curve, see Fig. 13-A; therefore, G^* is 133.3 J/m^2 and 200 J/m^2 for the reference and modified samples, respectively. Hence, the fatigue resistance in the modified specimen is 1.5 times higher than the reference one.

6. SEM micrographs

6.1. Quasi-static test

SEM micrographs of the fractured surfaces are illustrated in Fig. 14, for the reference, and Fig. 15, for the nanomodified laminates. Fig. 14-A shows the area near the initial crack tip. As seen, matrix cracking is the dominant damage mechanism because of the resin-rich area. With increasing the crack propagation, the fiber bridging phenomenon appears; so the fracture surface becomes rougher compared to the last stage (onset of crack growth) (Fig. 14-B). “Scarp” is one of the most important phenomena during matrix failure. When a local fracture starts along with a defect and spreads into the matrix, consider convergence between two adjacent crack planes. Some sharp steps can be formed at the boundary between these planes, which called a scarp. As seen in Fig. 14-C, many scarps were produced in the reference laminates while as it will be shown in the nanomodified laminates, nanofibers stopped occurring this phenomenon.

Unlike the reference laminate, carbon fibers or their imprints are not visible in the fracture surface of the modified samples. On the other hand, no bridging occurred by carbon fibers. As the curing temperature

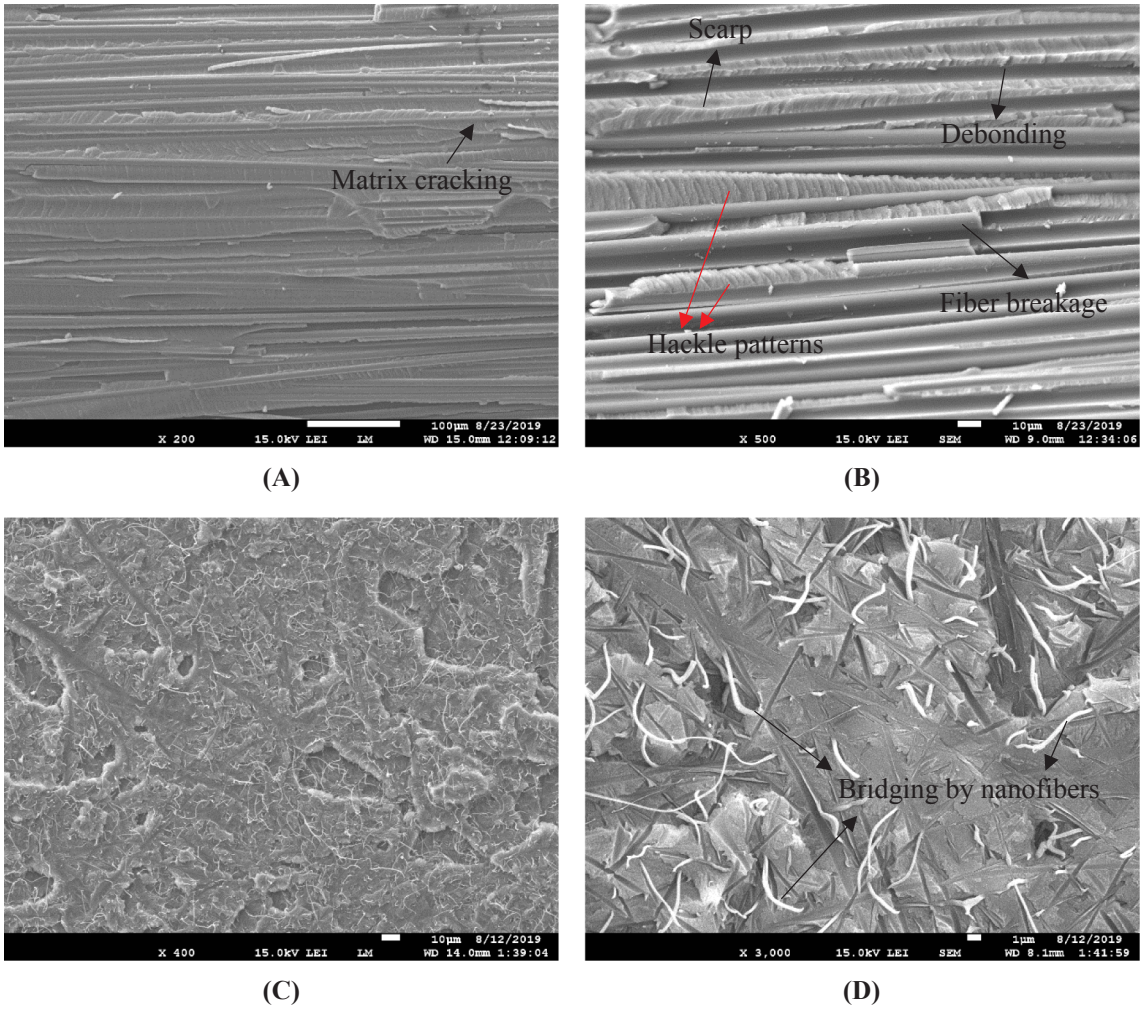

Fig. 16. The SEM micrographs of fractured surface under fatigue loading, (A) and (B) subjected to reference specimen, (C) and (D) subjected to nanomodified specimen. (For interpretation of the references to colour in this figure legend, the reader is referred to the web version of this article.)

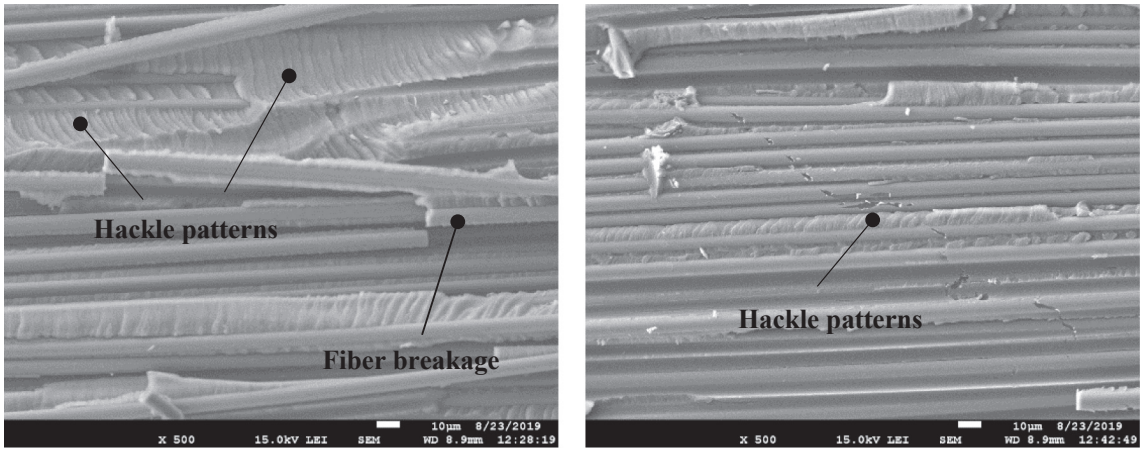

A) Δa =1mm & G_{Imax} = 134 J/m^2 **B)** Δa = 6mm & G_{Imax} = 87 J/m^2

$$\frac{da}{dN} = 1.76E^{-6} m/cycle \qquad \frac{da}{dN} = 1.64E^{-8} m/cycle$$

Fig. 17. The fracture surface of the reference specimen in different distance from the initial crack tip.

was less than melting point of nylon 66 (260 °C), the nanofibers maintained their initial configuration. Therefore, crack propagated between nanofibrous mats and the toughening mechanism is the bridging of nanofibers between upper and down layers. An important point is: if the modified laminates is in a situation in where the enviromental temperature is more than T_g temperature of nylon 66, it will be possile to decerease the effectiveness of nanofibers on thoughening the laminate. Because the nanofibers will have a rubbery behaviour; so will not be able to make bridge as strong as normal condition.

As can be seen in Fig. 15-A and B, the fracture surface of modified specimens is rougher and there are some insular areas at the surface. It means crack was deviated and its direction changed continuously between these insulars. As the route passed by the crack is longer than the reference, more energy is required; so the fracture toughness increased [48]. Another mechanism of toughening is plastic deformation of nanofibers during the failure. Fig. 15-C and D show the broken nanofibers. The rounded area at the fractured part proves the severe plastic deformation of nanofibers during failure. Therefore, more energy dissipated by the deformation of nanofibers and then increase fracture toughness.

6.2. Fatigue test

SEM micrographs subjected to fatigue tests are depicted in Fig. 16 and Fig. 17 for the reference and modified specimens, respectively. By comparing Fig. 16-A and Fig. 14-B (200× magnification), it can be concluded that the fracture surface of specimen tested under fatigue loading is generally smoother than quasi-static one. As seen in Fig. 16-B, the damage mechanisms such as fiber breakage due to bridging phenomena, fiber/matrix debonding, and scarp are also occurred during fatigue loading (like quasi-static test). However, some regular hackle patterns due to cyclic loading conditions were created at the fractured surface while there were very limited number ones under quasi-static test.

Fig. 16-C and D illustrate the SEM micrographs for nanomodified specimens subjected to fatigue test. According to Fig. 16-C and Fig. 15-A (400× magnification), the fatigue surface is again smoother than quasi-static one. Unlike the reference sample, the regular hackle patterns did not exist because of nanofiber bridging between matrix cracks. Bridging by nanofibers is visible at Fig. 16-D. The toughening mechanism in fatigue loading is similar to the quasi-static loading.

As seen in Fig. 9-A and B, the crack growth rate (da/dN) and the strain energy release rate (G_{max}) were decreased with increasing cycles. Fig. 17 depicts the fracture surface of the reference specimen. In order to study the effect of the strain energy release rate on damage features, SEM images were taken at different distances (Δa) from the initial crack tip. By knowing the actual crack length ($a_o + \Delta a$) at each point, the strain energy release rate (G_{max}) and the crack growth rate (da/dN) are available. As seen in this figure, by decreasing G_{Imax}, and da/dN, the size and the height of hackle patterns became smaller; so, the fractured surface was smoother. It should be noted that the morphology of the fractured surface in the nanomodified laminates did not change considerably during crack propagation because of covering by nanofiber.

7. Conclusion

In this study, the influence applying nylon 66 nanofibers on fatigue and fracture behavior of carbon/epoxy laminates is investigated. In the first step, the nanofibrous mat was interleaved between mid-layers of the laminate, then mode-I quasi-static and cyclic loadings were conducted under load-displacement condition. The fatigue tests were done with the same ratio of displacement ($\delta_{min}/\delta_{max} = 0.3$) and three various G_{Iimax}/G_{IC} (0.5, 0.7, 0.8). The following results can be concluded:

1. The results showed that mode-I fracture toughness of AS4/8552 laminates increased 133% using nylon 66 nanofibers.
2. The general fatigue graphs were plotted and observed that crack growth rate and the slope of $da/dN - \Delta G$ significantly decreased in the nanomodified specimens.
3. The threshold energy release rate (G_{Ith}) was obtained from the extrapolation method. It was found that G_{Ith} is 79.67 J/m^2 and 182.15 J/m^2 for the reference and modified specimens (128% increase).
4. G^*, physical strain energy release rate, a method based on energy balance was used to assess fatigue resistance of test samples. The outcomes showed that fatigue resistance at modified specimens is 1.5 times higher in comparison with the reference ones.
5. Considering fractured surface of the specimens using SEM micrographs proved that nanofibers improved the mechanical properties by means of 1- bridging between layers at the crack tip, 2- formation of insular areas at the process zone and increase the surface roughness 3- severe plastic deformation of nanofiber because of their thermoplastic behavior.
6. Nanofibers could decrease the main damages that occurred in the reference specimens such as fiber breakage, fiber-imprint, cusps, and scarps patterns.

CRediT authorship contribution statement

Reza Mohammadi: Validation, Formal analysis, Investigation, Data curation, Writing - original draft, Visualization, Writing - review & editing. **Mehdi Ahmadi Najafabadi:** Supervision, Resources, Project administration, Funding acquisition, Writing - review & editing. **Hamed Saghafi:** Conceptualization, Investigation, Resources, Writing - original draft, Project administration, Writing - review & editing. **Dimitrios Zarouchas:** Supervision, Resources, Project administration, Funding acquisition, Writing - review & editing.

Declaration of Competing Interest

The authors declare that they have no known competing financial interests or personal relationships that could have appeared to influence the work reported in this paper.

References

[1] Moallemzadeh AR, Sabet SAR, Abedini H, Saghafi H. Investigation into high velocity impact response of pre-loaded hybrid nanocomposite structure. Thin-Walled Struct 2019;142:405–13.
[2] Akangah P, Lingaiah S, Shivakumar K. Effect of Nylon-66 nano-fiber interleaving on impact damage resistance of epoxy/carbon fiber composite laminates. Compos Struct 2010;92(6):1432–9.
[3] Qian X, Kravchenko OG, Pedrazzoli D, Manas-Zloczower I. Effect of polycarbonate film surface morphology and oxygen plasma treatment on mode I and II fracture toughness of interleaved composite laminates. Compos A Appl Sci Manuf 2018;105:138–49.
[4] Guo M, Liu L. Structuring the thermoplastic interleaf with lotus-leaf-like structure and its interlaminar toughening for CFRPs. Compos Sci Technol 2019;183:107825.
[5] Woo EM, Mao KL. Evaluation of interlaminar-toughened poly(etherlmide)-modified epoxy/carbon fiber composites. Polym Compos 1996;17(6):799–805.
[6] Dzenis YA, Reneker DH. Delamination resistant composites prepared by small diameter fiber reinforcement at ply interfaces. US Patent: 6265333; 2001.
[7] Li G, Li P, Zhang C, Yu Y, Liu H, Zhang S, et al. Inhomogeneous toughening of carbon fiber/epoxy composite using electrospun polysulfone nanofibrous membranes by in situ phase separation. Compos Sci Technol 2008;68(3):987–94.
[8] Magniez K, De Lavigne C, Fox BL. The effects of molecular weight and polymorphism on the fracture and thermo-mechanical properties of a carbon-fibre composite modified by electrospun poly (vinylidene fluoride) membranes. Polymer 2010;51(12):2585–96.
[9] Zheng N, Huang Y, Liu H-Y, Gao J, Mai Y-W. Improvement of interlaminar fracture toughness in carbon fiber/epoxy composites with carbon nanotubes/polysulfone interleaves. Compos Sci Technol 2017;140:8–15.
[10] Cai S, Li Y, Liu H-Y, Mai Y-W. Effect of electrospun polysulfone/cellulose nanocrystals interleaves on the interlaminar fracture toughness of carbon fiber/epoxy composites. Compos Sci Technol 2019;181:107673.
[11] Zhang H, Bharti A, Li Z, Du S, Bilotti E, Peijs T. Localized toughening of carbon/epoxy laminates using dissolvable thermoplastic interleaves and electrospun fibres. Compos A Appl Sci Manuf 2015;79:116–26.
[12] Saghafi H, Moallemzadeh AR, Zucchelli A, Brugo TM, Minak G. Shear mode of

fracture in composite laminates toughened by polyvinylidene fluoride nanofibers. Compos Struct 2019;227:111327.
[13] Saghafi H, Ghaffarian S, Brugo T, Minak G, Zucchelli A, Saghafi H. The effect of nanofibrous membrane thickness on fracture behaviour of modified composite laminates–A numerical and experimental study. Compos B Eng 2016;101:116–23.
[14] Cheng C, Chen Z, Huang Z, Zhang C, Tusiime R, Zhou J, et al. Simultaneously improving mode I and mode II fracture toughness of the carbon fiber/epoxy composite laminates via interleaved with uniformly aligned PES fiber webs. Compos A Appl Sci Manuf 2020;129:105696.
[15] Beckermann GW, Pickering KL. Mode I and Mode II interlaminar fracture toughness of composite laminates interleaved with electrospun nanofibre veils. Compos A Appl Sci Manuf 2015;72:11–21.
[16] Barzoki PK, Latifi M, Rezadoust AM. The outstanding effect of nanomat geometry on the interlaminar fracture toughness behavior out of autoclave made glass/phenolic composites under mode-I loading. Eng Fract Mech 2019;205:108–19.
[17] Barzoki PK, Rezadoust AM, Latifi M, Saghafi H, Minak G. Effect of nanofiber diameter and arrangement on fracture toughness of out of autoclave glass/phenolic composites – experimental and numerical study. Thin-Walled Struct 2019;143:106251.
[18] Yuan B, Ye M, Hu Y, Cheng F, Hu X. Flexure and flexure-after-impact properties of carbon fibre composites interleaved with ultra-thin non-woven aramid fibre veils. Compos A Appl Sci Manuf 2020;131:105813.
[19] van der Heijden S, Daelemans L, Meireman T, De Baere I, Rahier H, Van Paepegem W, et al. Interlaminar toughening of resin transfer molded laminates by electrospun polycaprolactone structures: effect of the interleave morphology. Compos Sci Technol 2016;136:10–7.
[20] van der Heijden S, Daelemans L, De Schoenmaker B, De Baere I, Rahier H, Van Paepegem W, et al. Interlaminar toughening of resin transfer moulded glass fibre epoxy laminates by polycaprolactone electrospun nanofibres. Compos Sci Technol 2014;104:66–73.
[21] Daelemans L, Kizildag N, Van Paepegem W, D'Hooge DR, De Clerck K. Interdiffusing core-shell nanofiber interleaved composites for excellent Mode I and Mode II delamination resistance. Compos Sci Technol 2019;175:143–50.
[22] Wang Y, Wang Y, Wan B, Han B, Cai G, Chang R. Strain and damage self-sensing of basalt fiber reinforced polymer laminates fabricated with carbon nanofibers/epoxy composites under tension. Compos A Appl Sci Manuf 2018;113:40–52.
[23] Bortz DR, Merino C, Martin-Gullon I. Mechanical characterization of hierarchical carbon fiber/nanofiber composite laminates. Compos A Appl Sci Manuf 2011;42(11):1584–91.
[24] Chen Q, Zhang L, Rahman A, Zhou Z, Wu X-F, Fong H. Hybrid multi-scale epoxy composite made of conventional carbon fiber fabrics with interlaminar regions containing electrospun carbon nanofiber mats. Compos A Appl Sci Manuf 2011;42(12):2036–42.
[25] Hsiao K-T, Scruggs AM, Brewer JS, Hickman GJS, McDonald EE, Henderson K. Effect of carbon nanofiber z-threads on mode-I delamination toughness of carbon fiber reinforced plastic laminates. Compos A Appl Sci Manuf 2016;91:324–35.
[26] Ravindran AR, Ladani RB, Wang CH, Mouritz AP. Synergistic mode II delamination toughening of composites using multi-scale carbon-based reinforcements. Compos A Appl Sci Manuf 2019;117:103–15.
[27] Gholizadeh A, Najafabadi MA, Saghafi H, Mohammadi R. Considering damages to open-holed composite laminates modified by nanofibers under the three-point bending test. Polym Test 2018.
[28] Saghafi H, Fotouhi M, Minak G. Improvement of the impact properties of composite laminates by means of nano-modification of the matrix—a review. Appl Sci 2018;8(12):2406.
[29] Hamer S, Leibovich H, Green A, Avrahami R, Zussman E, Siegmann A, et al. Mode I and Mode II fracture energy of MWCNT reinforced nanofibrilmats interleaved carbon/epoxy laminates. Compos Sci Technol 2014;90:48–56.
[30] Daelemans L, Cohades A, Meireman T, Beckx J, Spronk S, Kersemans M, et al. Electrospun nanofibrous interleaves for improved low velocity impact resistance of glass fibre reinforced composite laminates. Mater Des 2018;141:170–84.
[31] Saghafi H, Zucchelli A, Palazzetti R, Minak G. The effect of interleaved composite nanofibrous mats on delamination behavior of polymeric composite materials. Compos Struct 2014;109:41–7.
[32] Gholizadeh A, Najafabadi MA, Saghafi H, Mohammadi R. Considering damage during fracture tests on nanomodified laminates using the acoustic emission method. Eur J Mech-A/Solids 2018.
[33] Brugo T, Palazzetti R. The effect of thickness of Nylon 6,6 nanofibrous mat on Modes I-II fracture mechanics of UD and woven composite laminates. Compos Struct 2016;154:172–8.
[34] Ahmed H, Shivakumar K. Enhancement of impact performance of AS4/3501-6 carbon/epoxy composite laminates by Nylon-66 nanofiber. Proceedings of the American Society for Composites—Thirty-second Technical Conference; 2017.
[35] Saghafi H, Minak G, Zucchelli A, Brugo TM, Heidary H. Comparing various toughening mechanisms occurred in nanomodified laminates under impact loading. Compos B Eng 2019;174:106964.
[36] Polat S, Avcı A, Ekrem M. Fatigue behavior of composite to aluminum single lap joints reinforced with graphene doped nylon 66 nanofibers. Compos Struct 2018;194:624–32.
[37] Brugo TM, Minak G, Zucchelli A, Saghafi H, Fotouhi M. An Investigation on the fatigue based delamination of woven carbon-epoxy composite laminates reinforced with polyamide nanofibers. Procedia Eng 2015;109:65–72.
[38] Brugo T, Minak G, Zucchelli A, Yan XT, Belcari J, Saghafi H, et al. Study on Mode I fatigue behaviour of Nylon 6,6 nanoreinforced CFRP laminates. Compos Struct 2017;164:51–7.
[39] Alessi S, Di Filippo M, Dispenza C, Focarete ML, Gualandi C, Palazzetti R, et al. Effects of Nylon 6,6 nanofibrous mats on thermal properties and delamination behavior of high performance CFRP laminates. Polym Compos 2015;36(7):1303–13.
[40] Papadopoulou EL, Pignatelli F, Marras S, Marini L, Davis A, Athanassiou A, et al. Nylon 6,6/graphene nanoplatelet composite films obtained from a new solvent. RSC Adv 2016;6(8):6823–31.
[41] HexPly® 8552 Epoxy matrix (180°C/356°F curing matrix) in FTA 072e. In: Publication HC, editor; 2013.
[42] ASTM D5528-13, Standard Test Method for Mode I Interlaminar Fracture Toughness of Unidirectional Fiber-Reinforced Polymer Matrix Composites, ASTM International, West Conshohocken, PA; 2013.
[43] ASTM D6115-97(2019), Standard Test Method for Mode I Fatigue Delamination Growth Onset of Unidirectional Fiber-Reinforced Polymer Matrix Composites, ASTM International, West Conshohocken, PA; 2019.
[44] ASTM E647-15e1, Standard Test Method for Measurement of Fatigue Crack Growth Rates, ASTM International, West Conshohocken, PA; 2015.
[45] Panduranga R, Shivakumar K. Mode-II total fatigue life model for unidirectional IM7/8552 carbon/epoxy composite laminate. Int J Fatigue 2017;94:97–109.
[46] Alderliesten RC, Brunner AJ, Pascoe JA. Cyclic fatigue fracture of composites: What has testing revealed about the physics of the processes so far? Eng Fract Mech 2018;203:186–96.
[47] Amaral L, Zarouchas D, Alderliesten R, Benedictus R. Energy dissipation in mode II fatigue crack growth. Eng Fract Mech 2017;173:41–54.
[48] Li P, Liu D, Zhu B, Li B, Jia X, Wang L, et al. Synchronous effects of multiscale reinforced and toughened CFRP composites by MWNTs-EP/PSF hybrid nanofibers with preferred orientation. Compos A Appl Sci Manuf 2015;68:72–80.